Available online at www.sciencedirect.com
SCIENCE DIRECT
Polymer 46 (2005) 9043–9052
polymer
www.elsevier.com/locate/polymer

Film formation, surface character, and relative density for electrochromic PEI/(PSS:PEDOT) multilayered thin films

Zhexiong Tang[a], Sean T. Donohoe[a], Jeanne M. Robinson[b], Peter A. Chiarelli[a,c,*], Hsing-Lin Wang[a,*]

[a]*Biosciences Division, Los Alamos National Laboratory, Los Alamos, NM 87545, USA*
[b]*Chemistry Division, Los Alamos National Laboratory, Los Alamos, NM 87545, USA*
[c]*Faculty of Clinical Medicine, Oxford University, Oxford OX1-3JA, UK*

Received 9 April 2005; received in revised form 25 June 2005; accepted 7 July 2005
Available online 8 August 2005

Abstract

Thin films of alternating layer composition were constructed from the polyelectrolyte complex PEDOT:PSS and the polycation PEI, using ionic self assembly (ISA). The PEI/PEDOT:PSS system displays a consistent trend in film growth, as evidenced by UV–visible spectroscopy and ellipsometry. We find that the overall density of PEDOT increases with increasing number of layers. The density of PSS during multilayer deposition differs from PEDOT, with a sharp drop in density between the 3rd and 6th bilayers. Combining film deposition estimates with contact angle measurement, we distinguish three regions of growth, separated by the 3rd and 6th layers. We ascertain that a constant level of interpenetration between PEI and PEDOT:PSS is reached by the 6th layer. Results from kinetics experiments and pH variation reveal a local increase in pH for the PEDOT species as it comes into contact with the PEI surface. Electrochemical characterization indicates that our films have an interpenetrated PEDOT network and a relatively hydrophilic surface. We demonstrate that ISA can be used to generate robust thin films, stable over a large pH range, whose coloration and conductivity may be manipulated on a large scale using applied voltage, and may be fine-tuned by changing the pH. The films exhibit electrochromic properties similar to other PEDOT derivatives, with a change in transmittance of 51% for 16 bilayers at 643 nm.

Keywords: Polyelectrolyte; Electrochromic; Self-assembly

1. Introduction

Conducting polymer thin films have shown great promise in the field of optical electronics, demonstrating applications over a wide range of technologies including light detection [1], microcavity lasing [2], electrochromic display [3], light emitting diodes [4], optical switching [5], and optical computing [6]. Specifically, the ability for many polymeric materials to undergo coupled alterations in optoelectronic properties due to chemical or electrical perturbations of redox state lend to them unique advantages within the field of functional materials engineering [7–9]. Polymeric materials possess substantial tensile strength, may be inexpensively processed, and may retain their optoelectronic stability over a long period of time. Furthermore, many such materials have considerable water solubility, facilitating assembly into multilayered architectures [10,11]. Well known examples of polymers with such diverse function include polyaniline [12], poly(3,4-ethylenedioxythiophene) (PEDOT) [13–16], and poly(*p*-phenylene vinylene) [17,18].

PEDOT has been well studied within the field of conducting polymers over the past decade [19–23]. PEDOT is stable, easily oxidized, and has a structure lacking undesired α,β- and β,β-couplings within the polymer backbone. PEDOT films have a very high conductivity (>200 S/cm) [24], and display switchable optical absorbance when converted from the reduced to the oxidized state. By introducing the water soluble polyelectrolyte poly(styrene sulfonate) (PSS) as a counterion dopant during polymerization, a PEDOT:PSS complex has been

* Corresponding authors. Tel.: +1 505 667 9944.
E-mail addresses: peter.chiarelli@linacre.ox.ac.uk (P.A. Chiarelli), hwang@lanl.gov (H.-L. Wang).

0032-3861/$ - see front matter © 2005 Elsevier Ltd. All rights reserved.
doi:10.1016/j.polymer.2005.07.023

generated, showing high water solubility. This dual-polymer complex formed a highly stable dispersion in water, with substantial conductivity (~10 S/cm), high visible light transmissivity, and robust film formation properties [25,26]. Since PEDOT:PSS can switch color (opaqueness) through changes of oxidation potential, polyelectrolyte thin films incorporating PEDOT:PSS show promise for electrochromic and optoelectronic technologies such as flexible displays and smart windows [27,28].

Popular thin film deposition methods for polyelectrolytes include electropolymerization [29], spin-assembly [30–32], ionic self-assembly [33–35] and surface polymerization by chemical means [36]. Ionic self-assembly (ISA) is an ideal technique for the adsorption of electroactive polyelectrolytes, as it allows substantial control over film design and resulting molecular architecture [33,37–40]. A charged substrate is alternately dipped into dilute aqueous solutions of polycation and polyanion, depositing layers with specific thickness and composition. Homogeneous, electronically conductive ISA films have been fabricated, including assembly schemes containing the PEDOT:PSS composite [27,28].

In this work, we assemble thin films in a scheme of alternating charge using a PEDOT:PSS colloidal dispersion (Baytron P) as the polyanion and poly(ethylenimine) (PEI) as the polycation (Fig. 1). The challenge we faced in working with this system is that PEI is insulating and once it was used as a binder between PEDOT:PSS layers, it prevented electrochemical accessibility throughout the films. This presents a serous limitation of using PEDOT:PSS/PEI for the development of optoelectronic devices. A natural solution to this problem is to reduce the thickness of the PEI layer by lower the PEI concentration used for thin film deposition. By doing so, we have demonstrated a way to prepare PEDOT:PSS/PEI thin films with full electrochemical accessibility throughout the films. We can rationalize the above results as interpenetration between layers is responsible for establishing connection between PEDOT:PSS layers. The effects of interpenetration/film formation can be realized through the study of surface character, morphology, and relative layer density. Overall, we have achieved a greater understanding of film deposition using the self-assembly method that would allow further development of functional thin films, not limited to one single material or device.

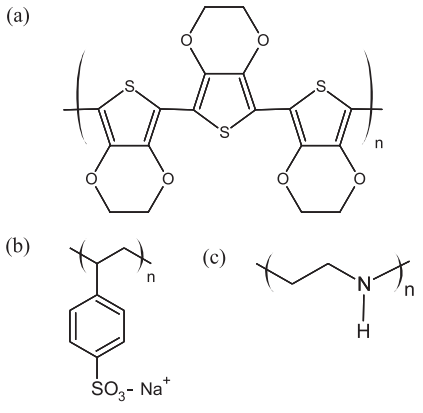

Fig. 1. Molecular structure for (a) PEDOT, (b) PSS, and (c) PEI.

2. Experimental section

2.1. Materials

The branched polycation, poly(ethylenimine) (PEI; average molecular weight 25,000) and the polyanion poly(acrylic acid) (PAA; average molecular weight 90,000) were purchased from Aldrich and Acros, respectively, and used as received. The polymer composite Baytron P, consisting of 3,4-poly(ethylenedioxythiophene) (PEDOT) and poly(styrenesulfonate) (PSS) was purchased from Starck. PEDOT is partially oxidized to allow complex with PSS, however, the exact oxidation state of DEDOP is unknown. PEI was diluted to 1 mM concentrations using ultrapure distilled water (resistivity $\geq$18 MΩ/cm). The pH value of PEI solution is ~8.0. The PEDOT:PSS solution was diluted to 50, 5 and 0.5 mM, respectively, using ultrapure water and the pH values 2.5, 3.5 and 4.2, respectively.

2.2. Substrate preparation

Substrates for polyelectrolyte deposition included Fisherfinest glass microscope slides, 2 in. round single-side polished silicon wafers (Silicon Sense, Inc.), 3 in. Fused Silica plates (Sierra Precision Optics), and ITO (indium tin oxide) coated glass slides with 8–12 MΩ/cm resistance (Aldrich). Prior to film formation, fresh substrates were sonicated for 10 min in ethanol or acetone, Ar plasma cleaned (Harrick model PDC-32G.) for 5 min to expose an oxide surface, and stored in ultrapure water.

2.3. Film assembly

Multilayered thin films were constructed by ionic self-assembly (ISA), alternately immersing a substrate in polyelectrolyte solutions of opposite charge for 5 min each. After deposition of each layer, the substrate was washed four times with water. Prior to measurement, substrates were dried with a stream of N_2.

Ex situ deposition kinetics experiments for PEDOT:PSS were performed by immersing the substrate in PEDOT:PSS solution for specified time intervals, and characterizing the thin film after each period of deposition. Prior to investigation of kinetics at a given layer, a number of underlying layers were constructed, also by ISA.

2.4. UV–visible characterization

UV–vis–NIR measurements of the multilayered films built on glass and fused silica were obtained using a Varian Cary 500 spectrophotometer. PEDOT:PSS has a broad absorbance profile with peaks at ~195, ~225, and ~240 nm due to PSS, and a peak at ~930 nm due to PEDOT. Investigation of the adsorption profile dependence on pH for PEDOT:PSS involved immersing a pre-constructed film in solutions of varying pH (1.05, 3.20, 5.61, 8.18, 9.63, 11.01, 12.0) for 5 min each, rinsing the substrate in two beakers of ultrapure water, and acquiring a spectrum for the film at each pH. Solution pH values were adjusted using either ammonium hydroxide or hydrochloric acid.

Relative density estimation for PEDOT and PSS was performed by dividing PEDOT:PSS ellipsometric thickness by the UV–visible absorbance value at λ_{max} for either PEDOT or PSS (930 or 225 nm, respectively). Ellipsometric data were pre-analyzed by determining the contributions to film thickness of PEDOT:PSS alone (subtraction of preceding PEI-terminated film thickness from each PEDOT:PSS-terminated film thickness, and summing over all PEDOT:PSS thickness contributions up to the desired layer).

2.5. Ellipsometric measurement

Ellipsometric measurements were collected on a Rudolph Research AutoEL III single-wavelength null-ellipsometer and a Rudolph Research Manual Photoelectric Ellipsometer. 1″ round single-side-polished silicon wafers were used as substrates for films characterized by ellipsometry. Data was collected at a beam incidence angle of 70° and a wavelength of 632.8 nm. Thickness measured using single-wavelength ellipsometry is considered valid under the assumption that absorbance—incorporated in the ellipsometry model as the imaginary component of the refractive index—has minimal impact on the ellipsometric calculation, as long as very low (~within the first delta/psi cycle) thicknesses are being measured. Refractive index of $1.5+0i$ was used to manually calculate ellipsometric film thicknesses from Δ and Ψ parameters [41]. Measurements of the native SiO_2 layer were subtracted from film measurements to determine total ellipsometric film thickness.

2.6. Microscopy and contact angle methods

Atomic force microscopy (AFM) images were collected from films constructed on silicon wafers, using a Nanoscope IIIa (Digital Instruments) in tapping mode.

Optical microscopy images were obtained at 20× magnifications using a (Olympus BH-2-UMA scope with polarizers) coupled to a CCD detector. Thin films observed using optical microscopy were also constructed on polished silicon substrates.

Surface contact angle measurements were obtained with a Tantec CAM-wafer II optical goniometer with CCD camera, using the half-angle method of measurement.

2.7. Electrochemical methods

Cyclic voltamograms were collected using a three-electrode single-compartment cell—with ITO glass coated by polyanion and polycation layers as the working electrode, a bare platinum plate as the counter electrode, and Ag/AgCl as the reference electrode. Tetrabutylammonium hexafluorophosphate (0.2 M) in acetonitrile was used as the electrolyte.

UV–visible spectra were measured for the PEI/PEDOT:PSS multilayer thin films under different oxidation/reduction potential. Redox potentials were controlled using a CH Electrochemical workstation. Films deposited on ITO substrates were positioned in a quartz cell containing electrolyte, a platinum coil counter electrode, and an Ag/AgCl reference electrode.

3. Results and discussion

3.1. Quantitative measurement of film formation

Thin films of alternating layer composition were constructed from 1.0 mM PEI and 1.0 mM PEDOT:PSS by ionic self-assembly (ISA). Deposition of the first PEI layer onto the ITO substrate results from an electrostatic interaction between the positively charged PEI and the negatively charge oxide surface. Fig. 2(a) shows the absorption intensity for 15 bilayers constructed at native pH, with the absorbance at λ_{max} for PSS and PEDOT principle adsorption peaks plotted separately. These peaks have different relative heights, a consequence of the different molar absorptivity for PSS and PEDOT. The upward trends for PSS and PEDOT change concurrently, suggesting that PSS and PEDOT co-adsorb to the surface. In Fig. 2(a), the data from either peak is plotted on a scale where the absorbance at λ_{max} coincides for the 1st and 15th bilayers. The similarity of the two curves suggests that the energy of association between the two polyelectrolytes is substantially greater than the energy driving the absorption of either single member of the composite. However, we observe a small disparity in relative deposition between the two species. The results suggest that adsorption either of uncomplexed PEDOT or the deposition of complexed particles with an elevated PEDOT content occurs after the 4th bilayer, evidenced by the relative increase in amplitude of the PEDOT curve. We observe slow growth in deposition amount of both species for the first few bilayers, which gradually increases to a steady-state deposition amount around bilayers 4–6. Upon close inspection, the two curves

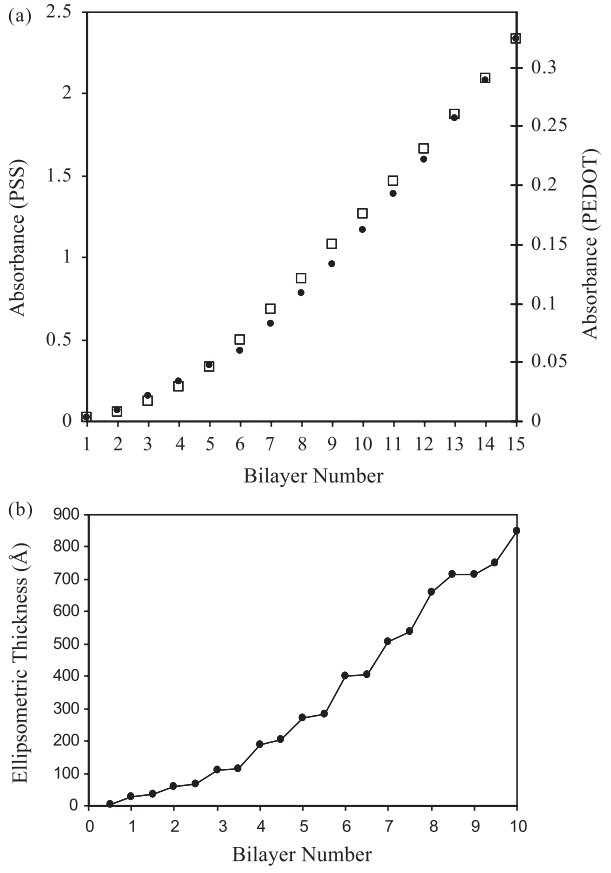

Fig. 2. (a) UV–visible absorbance at $\lambda_{max} \approx 275$ nm (●) and 930 nm (□) for 15 bilayers of 1 mM PEI/1 mM PEDOT:PSS. (b) Ellipsometric thickness obtained each layer for 10 bilayers of the same system.

show transitions between low and higher slopes at a different number of bilayers. The amount of PEDOT deposited in each bilayer (indicated by the slope of the absorbance curve) becomes enhanced around bilayer 4, whereas PSS shows a delayed change, near bilayer 6.

Ellipsometric thickness data for 1.0 mM PEI/1.0 mM PEDOT:PSS films demonstrate that the major change in thickness growth begins around the 2nd–3rd bilayer, corresponding to a thickness range of ~60–100 Å (Fig. 2(b)). The primary contributions to thickness of the system come from the PEDOT:PSS layers. We have previously demonstrated a bi-linear trend in ellipsometric thickness during the growth of multilayered films, in which the UV–visible signal changes linearly with layer number [23]. Our previous research [30,31] and the work of others [42] have suggested that substrate effects influence packing density of the first few layers. This trend has typically been observed around 50–80 Å in total film thickness.

To better understand the formation of a PEDOT:PSS mixed layer, we calculated the overall packing density of both species in the film, throughout the course of multilayer deposition. Our method utilized summation, at each layer, of the total UV–visible absorption either for PEDOT or PSS, and of the ellipsometric thickness components only corresponding to the PEDOT:PSS layer, thus eliminating potential confounds due to fluctuations in PEI layer thickness. We divide total ellipsometric thickness at each PEDOT:PSS layer by the total absorbance at λ_{max} due only to the appropriate species. In this manner, we obtain the quantity absorbance unit Å per for PEDOT and PSS (Fig. 3), which is proportional to density. Note that our technique observes only the total film density at a given bilayer, which will consist of an arrayed sum of the variable contributions from each constituent layer. A comparison of absolute density values between PEDOT and PSS is of limited utility, since differences in molar absorptivity yield separate scales for the two species. The value of our model emerges through its ability to identify trends in overall film density, and the data in Fig. 3 has been scaled to match PEDOT and PSS values from the 1st and 10th bilayers, for ease of comparison. The results suggest that total PEDOT density increases by ~30% between bilayers 1 and 2. From the second bilayer onward, we observe a relatively linear, slow increase in total PEDOT density. The PEDOT film density at the 10th bilayer is ~50% higher than the density of the first bilayer alone. PSS shows dissimilar behavior in total density. After increasing by ~38% between the first and 3rd bilayers, total PSS density drops precipitously between the 3rd and 6th bilayers, only to rise once again from the 6th bilayer onwards. These trends are rather surprising, and suggest that our polyelectrolyte thin films undergo dramatic changes in layer structure or morphology during the process of multilayer buildup. Moreover, the trend of increased density observed here in PEI/PEDOT:PSS films is different from the qualitative trends of we have formerly observed in ISA films. For instance, we have observed increased packing density in initial layers of poly[1-[4-(3-carboxy-4-hydroxyphenylazo)benzenesulfonamido]-1,2-ethanediyl, sodium salt] (PAZO) within the PEI/PAZO system [43].

Our density estimation method assumes that the PEDOT:PSS composite is well-mixed, lacking spatially segregated domains of either material. Potential overlap between individual absorption profiles of PEDOT and PSS represents a possible limitation to our model, although we expect that

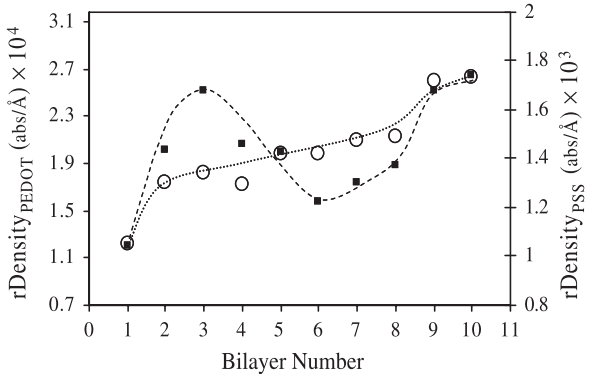

Fig. 3. Relative density (rDensity) for PEDOT (○) and pass PSS (■) within each PEDOT:PSS layer of 10 bilayer 1 mM PEI/1 mM PEDOT:PSS film.

such overlap is of limited impact, as we are not interested in absolute density, but rather the relative change in packing density. The comparative density investigation combining UV–visible measurements and ellipsometric layer thickness measurements, over the course of multilayered deposition, is extremely useful in understanding the formation mechanism of polyelectrolyte multilayer thin films and their structure-property relationships.

In a separate experiment, we attempted to assemble alternating layers of PEDOT:PSS with pure PSS (polyanion) and observed no adsorption of PEDOT:PSS to the film surface. This result shows that the PEDOT:PSS behaves as a polyanion, which is consistent with work from other groups [19,27,28].

3.2. Contact angle determination

We further investigated film formation dynamics using surface contact angle measurement at each layer of the PEI/PEDOT:PSS film (Fig. 4). It has been previously demonstrated that the hydrophobicity of surfaces with adsorbed polyelectrolyte layers can be tuned by altering the properties of the outermost layer [44]. Our PEDOT:PSS system shows three distinct regions of surface behavior—evidenced by the large negative slope between the 1st and 2nd bilayers, an intermediate slope between the 2nd and 6th bilayers, and a slope close to zero in following layers. Furthermore, we see a second effect, in which the contact angles for PEI and PEDOT:PSS surfaces diverge, and subsequently reconverge. Comparing to the 40° contact angle of bare PEI, the contact angle of bare PEDOT:PSS is only 20°. It is clear that the PEDOT:PSS-coated surface is more hydrophilic than the PEI surface. We see that the initial ITO surface is quite hydrophobic, with a large contact angle of ~85°. As the number of layers increases, there is an overall trend toward increased hydrophilicity, until a constant contact angle is reached. The constant contact angle beyond the 6th bilayer suggests that steady-state surface conditions for both the PEI and the PEDOT:PSS are attained. The similarity in contact angle between the two species probably derives from high interpenetration. Between bilayers 2 and 6, the contact angles are considerably different for PEI and PEDOT:PSS, and PEDOT:PSS presents a surface of considerably greater hydrophilicity than PEI. The discrete surface characteristics may be explained by increased segregation of the two polyelectrolytes, i.e. decreased interpenetration between layers. Temporal changes in static contact angles can also be due to rearrangement of fragments in the film that occur at the film-water interface upon contact with the water drop. As previously mentioned, we observe a reduction in PSS density between bilayers 2 and 6 of the film. A different relative PEDOT:PSS ratio in these layers could explain the disparity in surface behavior compared to the earliest layers and bilayers >7. Data from the first two bilayers, where the difference in contact angle between PEDOT:PSS and PEI is very small, suggests that non-uniform PEDOT:PSS adsorption occurs in this layer. We attribute the similarity in contact angle between PEI and PEDOT:PSS in the first two layers to sparse overall surface coverage, leading to intermixed islands of deposition. This result agrees well with low relative density measurements for both PEDOT and PSS in the first two layers.

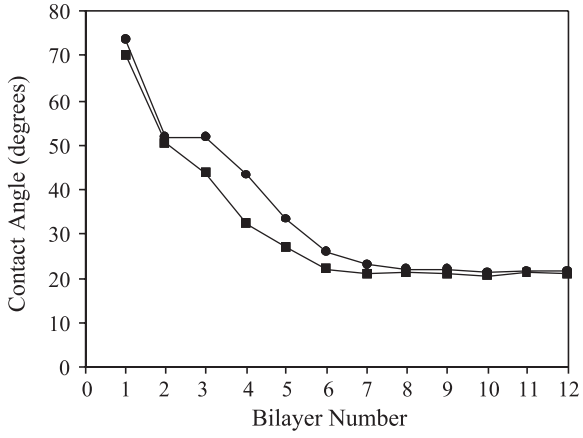

Fig. 4. Contact angle for PEI (●) and PEDOT:PSS (■) layers in a 10 bilayer 1 mM PEI/1 mM PEDOT:PSS film.

3.3. Deposition kinetics

We performed stopped-deposition kinetics experiments to monitor film growth on a substrate [43,45]. We first studied the adsorption of one single layer of PEDOT:PSS from solutions of varying concentration (50, 5 and 0.5 mM) (Fig. 5). PEDOT:PSS layers were adsorbed onto slides precoated with a single deposited layer of PEI (10 mM). For each curve, all points correspond to a common substrate, taken out of the PEDOT:PSS solution, washed, dried, measured, and placed back in solution to undergo further deposition. The total amount absorbed for one layer by this method is essentially the same as that for one layer adsorbed

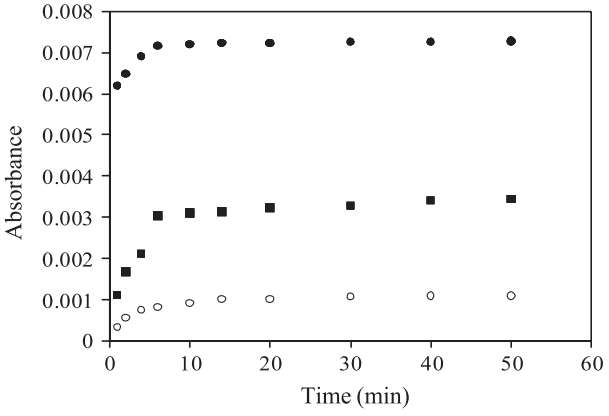

Fig. 5. Ex situ kinetics measurement during adsorption of PEDOT:PSS onto a single layer of PEI. UV–visible measurements were obtained at $\lambda_{max} \approx 930$ nm for PEDOT:PSS concentrations of 0.5 mM (○), 5 mM (■), and 50 mM (●).

from the same solution concentrations without interruption. Single-bilayer films deposited from solution concentrations corresponding to those used in multilayer film deposition reach saturation coverage around 5 min, confirming the utility of 5 min deposition times for achieving equilibrium surface conditions. Measurements made on samples immersed for long times (up to 24 h) show no significant additional adsorption. We find that the amount of deposited polymer depends strongly on the solution concentration, with higher concentrations resulting in greater amounts of adsorbed PEDOT:PSS at equilibrium.

Fig. 6(a) and (b) display the kinetic behavior for the formation of the fifth PEDOT:PSS layer, deposited from 0.005 M PEDOT:PSS solution. The 930 nm PEDOT peak (Fig. 6(a)) shows typical behavior for a polyelectrolyte thin film, with saturated coverage around 200 s. The delocalized polarons (charge carriers) are also monitored at 1700 nm (Fig. 6(b)), demonstrating a different trend, reaching a maximum value around 120 s and then subsequently decreasing in amplitude. Given the data from the 930 nm peak, we believe that this decline in the value at the 1700 nm peak is not due to detachment of PEDOT from the film surface, but instead due to a change of the local pH of attached PEDOT molecules.

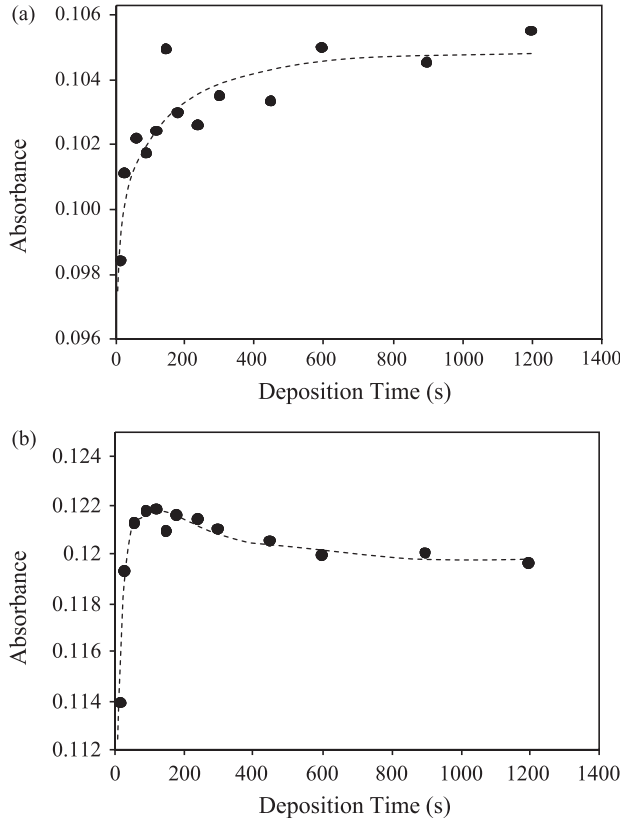

Fig. 6. Ex situ kinetics measurement at (a) 930 nm and (b) 1700 nm during adsorption of 1 mM PEDOT:PSS onto four complete bilayers of 1 mM PEI/1 mM PEDOT:PSS terminated with a single layer of PEI.

3.4. pH influence on film properties

To examine the effect of pH variation on the UV–visible absorbance profile of PEDOT:PSS, we constructed a 15 bilayer film on fused silica from PEI and PEDOT:PSS solutions at native pH and collected an absorption spectrum after submerging the film in solutions of each pH (1–12) (Fig. 7).

As pH is increased, the UV–visible absorption at 1700 nm drops significantly, with the greatest rate of attenuation occurring between pH values of 9–12. Above pH 12, the film detached from the substrate preventing measurement beyond this pH value. In agreement with our hypothesis for the kinetic data at 1700 nm, the absorbance value at this pH value changes to a much larger extent than the absorbance at 930 nm, and the absorbance at the two wavelengths varies inversely. An isosbestic point is observed at ~1010 nm. Recalling our kinetics experiment, the absorbance value at 1700 nm is shown to decrease after a local maximum, suggesting that the data above 120 s in Fig. 6(b) indicate an increase in local pH of PEDOT. Examining Fig. 6(a), we see no such drop in absorbance. This result has implications for the way we might view the dynamics of film formation. An increased basicity of the PEDOT molecule, as it leaves the solution phase and adsorbs to the solid surface, may arise from direct

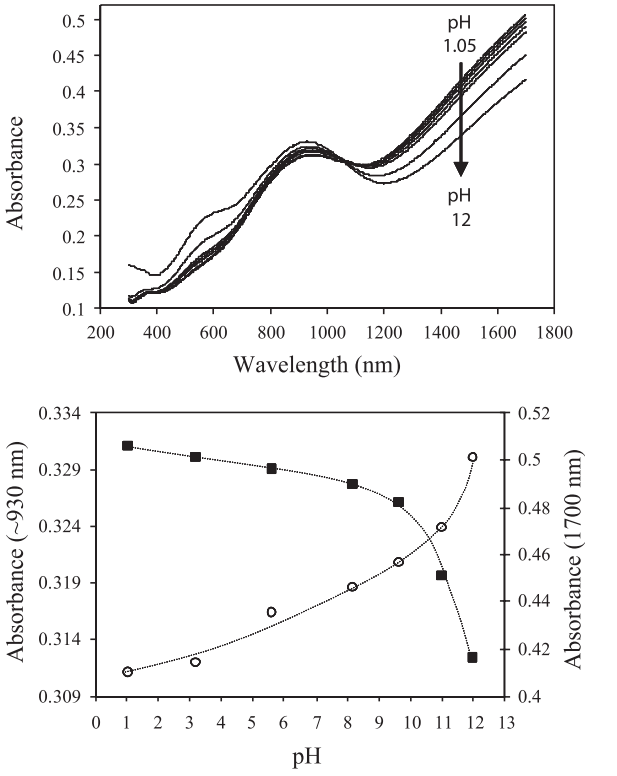

Fig. 7. (a) UV–visible spectra for a 15 bilayer 1 mM PEI/1 mM PEDOT:PSS film, immersed in solutions of variable pH (1.05, 3.20, 5.61, 8.18, 9.63, 11.01, 12.0). (b) UV–visible absorbance at ~930 nm (○) and 1700 nm (■) as a function of pH.

interaction with non-protonated amine groups of the PEI underlayer. PEI becomes protonated in solution to achieve a positive charge, and 10 mM PEI has a native solution pH of ~9.2. Our observations provide direct evidence of non-electrostatic interaction between the PEI layer and the PEDOT species.

3.5. Electrochemistry and spectroelectrochemistry

Cyclic voltammetry (CV) was used to identify redox potential ranges and investigate electrochemical behavior of PEDOT:PSS. We employed a considerable scanning range, between −1.0 and 0.8 V (vs Ag/AgCl), using a supporting electrolyte of 0.2 M tetrabutylammounium hexafluorophosphate in acetonitrile. PEI/PEDOT:PSS multilayered films were assembled onto ITO-coated glass substrate, and functioned as the working electrode. To evaluate the electrochemical accessibility of PEDOT within our films, the CV dependency on scan rate was examined. The CV characterization of 16 bilayer PEI/PEDOT:PSS films (Fig. 8(a)) shows a sharp redox wave appearing at −0.28 V (vs Ag/AgCl). This wave corresponds to the elimination and creation of distributed cationic polarons on the PEDOT polymer backbone. The amplitude of oxidative and reductive peaks increases with scan rate, from $\Delta E_p =$ 0.47 V at 0.02 V/s to $\Delta E_p = 0.61$ V at 0.1 V/s. This trend indicates that electron transfer from ITO to PEDOT occurs slowly, due to resistance of the inert PSS and PEI spacer layer. Oxidation and reduction peak heights scale linearly with the square root of scan rate. To further validate this relationship, we use a smaller electrolyte anion(tetrafluoroborate) to study the slow kinetics of ion diffusion. We plot the peak current as a function of square root of scan rate for both electrolyte anions, as shown in Fig. 8(b). The faster kinetics as indicated by the steeper slope and higher current for the tetrafluoroborate electrolyte anion confirm that smaller electrolyte anion indeed has a faster rate of diffusion.

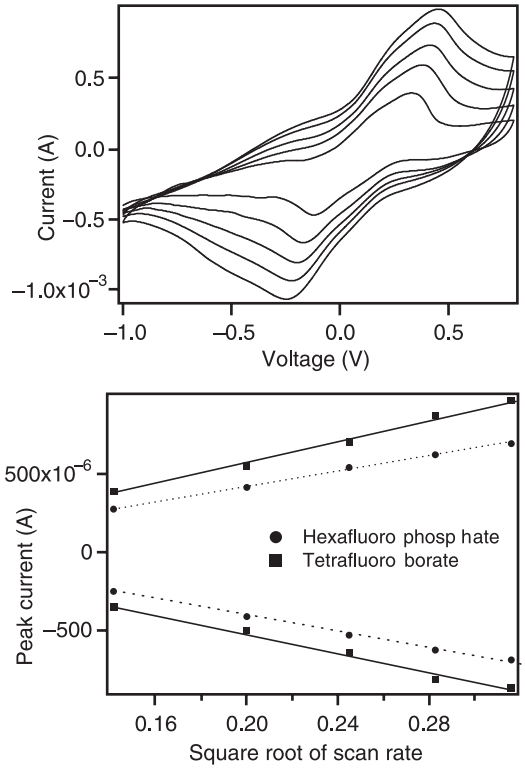

Fig. 8. (a) Cyclic voltammograms for 16 bilayers of 0.1 mM PEI/1 mM PEDOT:PSS. Scan were performed at 0.02, 0.04, 0.06, 0.08, and 0.1 V/s, using 0.2 M (TBA)4PF6 as the electrolyte and Ag/AgCl as the reference electrode. (b) Peak current of Oxidation and reduction curve vs square root of scan rate using 0.2 M (TBA)4PF6 and (TBA)4BF4 as electrolytes, respectively.

The optical properties of the electrochromic thin films were evaluated by measuring the changes of UV–visible spectra in situ. For this investigation, films assembled onto ITO substrates were inserted into a transparent electrochemical cell, where UV–visible spectra of the films were measured at different oxidation potentials. Our results are presented as a series of UV–visible absorbance curves correlated to various redox potentials for a 16 bilayer film (Fig. 9). The electrochemical scan was performed cathodically, proceeding from 1.0 to −0.8 V, with 3 min allowed for equilibration at each potential to minimize transient effects.

In the reduced state, the layers absorb strongly at 643 nm, corresponding to the dark blue, neutral form of PEDOT. At increasingly positive potentials, PEDOT is oxidized, introducing charge-carrying energy states between valence and conduction bands. The presence of these states shifts light absorption from the neutral peak to a new peak at 900 nm, and finally to the far infrared. The absorbance from 800 nm to the far infrared corresponds to the formation of polaron charge carriers, and bipolaron formation at high doping levels [19]. PEDOT in its oxidized state has a very weak absorbance from 350 to 750 nm (visible region) which

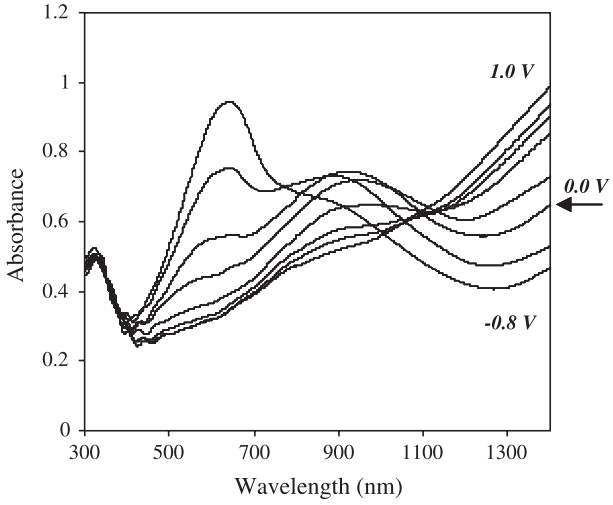

Fig. 9. UV–visible absorption spectra for 16 bilayers of 0.1 mM PEI/1 mM PEDOT:PSS, with applied potential varied over a range between −0.8 and +1.0 V (vs Ag/AgCl).

results in the pale blue/transparent color. This electrochromic effect for pure PEDOT is known and well understood [26]. However, incorporation of PEDOT:PSS into a multilayered structure using ionic self-assembly method as part of the electrochromic devices is only reported by DeLongchamp et al. [20,21]. Here, we demonstrate the full electrochromic effect in a single PEI/PEDOT:PSS multilayer system. This result suggests an interpenetrating PEDOT network within an insulated PSS and PEI matrix that allows for the color in all layers to change from dark blue to a highly transparent color. Fig. 10 shows the thin film transmission as a square wave potential between −0.8 and 1.0 V with an applied frequency of 0.25 Hz. To monitor the change in thin-film transmission at different oxidation states, we set the detector wavelength at 643 nm, which has a significant contrast in transmission between −0.8 and 1.0 V, to monitor the change in thin film transmission at different oxidation states and performance characteristics as electrochromic materials. Fig. 10 clearly shows the PEI/PEDOT:PSS thin film switching transmission from 80% at 1.0 V to 29% at −0.8 V. Variable coloration of PEI/PEDOT:PSS is demonstrated using digital images of the system at different potentials (Fig. 11).

3.6. Atomic force and light microscopy

Light microscope pictures obtained for 10 bilayers of 1 mM PEI/0.1 mM PEDOT:PSS deposited on a reflecting silicon surface are displayed in Fig. 12. The dramatic iridescence of this film supports the idea that our films display regions of different morphology. Such segregation of regions may be influenced by islands of deposition in early layers, mentioned previously in our discussion of contact angle. The iridescent pattern is thickness-dependent, and is not observed below ~6 bilayers (corresponding to ~400 Å in thickness).

A representative AFM image from a 1 bilayer PEI/PEDOT:PSS film is shown in Fig. 13(a) and (b). AFM of the surface confirms sparse coverage, in agreement

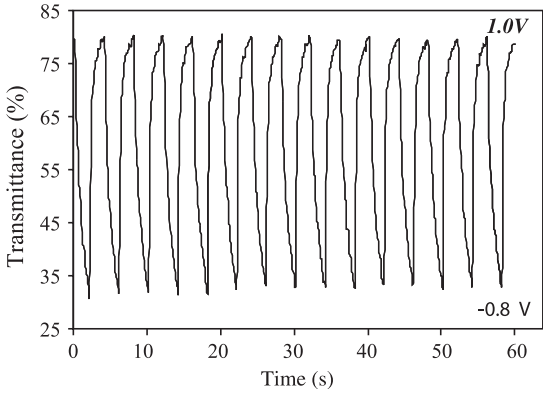

Fig. 10. Optical transmittance of a 16 bilayer 0.1 mM PEI/1 mM PEDOT:PSS film, monitored At 643 nm with cycled potential between −0.8 and 1.0 V.

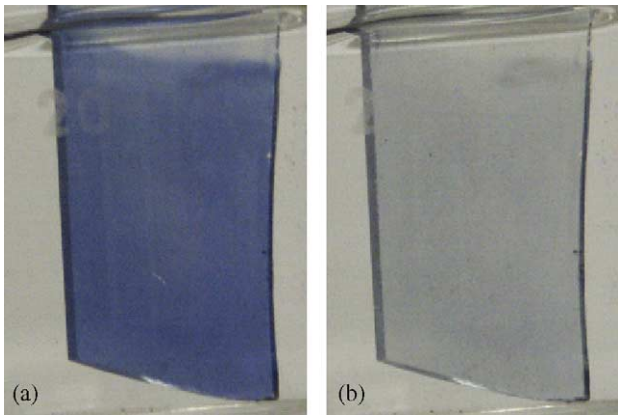

Fig. 11. Digital photographs for a 16 bilayer film of 1 mM PEI/1 mM PEDOT:PSS with applied potential of −0.8 V and (b) 1.0 V. The films as shown are immersed in 0.2 M (TBA)4PF6 acetonitrile solution within an electrochemical cell.

with our predictions based on contact angle measurements and UV–visible spectroscopy. Large regions of bare substrate are visible, and deposited material does not appear to possess any dominant shape or structure. Enhanced coverage of the first bilayer is not observed even with longer immersion times of the substrate in polyelectrolyte solution. Fig. 13(c) and (d) displays a representative AFM image from a 10 bilayer PEI/PEDOT:PSS film, showing large hills and valleys on the surface. We observe an average domain size of 200 nm for these broad features. The surface also appears to contain an array of small, spherical nanoparticles with a diameter of ~20 nm. These smaller particles are likely formed from associated PEDOT and PSS chains.

4. Summary

In this work, we have fabricated PEI/PEDOT:PSS multilayered thin films using ionic self-assembly. There is an initial nucleation of polyelectrolyte deposited on the glass surface for the first few bilayers. Complete surface coverage by the polyelectrolyte is not reached until the 6th bilayer, after which the amount of deposited polyelectrolyte

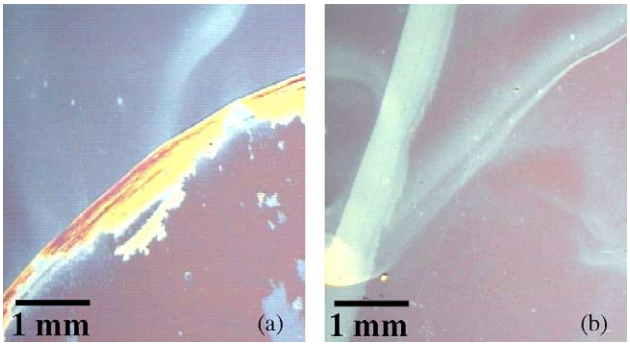

Fig. 12. Optical microscopy image for 10 bilayers of 1 mM PEI/0.1 mM PEDOT:PSS deposited on a Reflecting silicon surface. Images were obtained at 20× magnification.

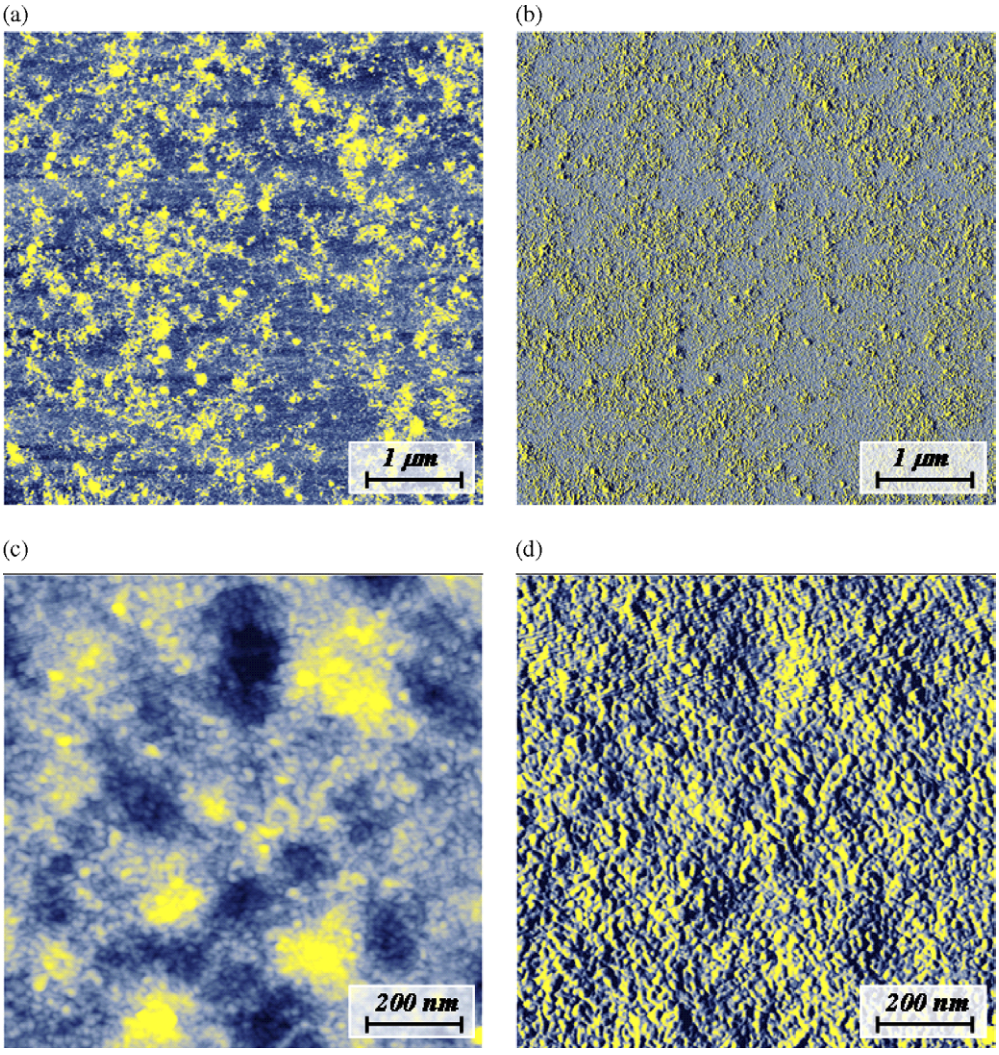

Fig. 13. (a) Height-data and (b) deflection-data AFM images for a 5 μm×5 μm area on a 1 bilayer 1 mM PEI/1 mM PEDOT:PSS film. (c) Height-data and (d) deflection-data AFM images for a 1 μm×1 μm area on a 10 bilayer film of the same composition. Both films were assembled on silicon substrates. The vertical scales of height are (a) 7 nm and (c) 25 nm. The vertical scales of deflection are (b) 0.29 V and (d) 0.15 V.

is reproducible. Contact angle results show that the hydrophobic ITO surface becomes more hydrophilic with increasing polyelectrolyte surface coverage, and reaches a constant value after the ~6th bilayer. The electrochemical accessibility of these multilayer thin films is well manifested by the cyclic voltammogram and the results show a diffusion limited redox mechanism. Interpenetration between two polyelectrolyte species results in formation of a PEDOT network throughout the whole film which is subject to electrochemical redox reactions and associated electrochromic properties.

Acknowledgements

The authors would like to acknowledge the financial support from the Cross Enterprise Technology Development Program of the National Aeronautics and Space Administration (NASA), the Laboratory Directed Research and Development (LDRD) fund of Los Alamos National Laboratory, and the Office of Science (DOE).

References

[1] Su M, Aslam M, Fu L, Wu NQ, Dravid VP. Appl Phys Lett 2004;84:4200–2.
[2] Tessler N, Denton GJ, Friend RH. Nature 1996;382:695–7.
[3] Monk PMS, Rosseinsky DR. Electrochromism: Fundamentals and applications. Weinheim: VCH inc; 1995.
[4] Burroughes JH, Bredley DDC, Brown AR, Marks RN, Mackay K, Friend RH, et al. Nature 1990;347:539–41.
[5] Kajzar F, Swalen JD, editors. Organic thin films for waveguiding nonlinear optics. Amsterdam: Gordon and Breach Publishers; 1996.
[6] Dubitsky Y, Zaopo A, Berendyaev V, Colombo M, Cortese M. Synth Met 2003;135/136:119–20.
[7] Sheats JR, Antoniadis H, Hueschen M, Leonard W, Miller J, Moon R, et al. Science 1996;273:884–8.
[8] Mikami T, Yanagi H. Appl Phys Lett 1998;73:563–5.

[9] Schlenoff JB, Laurent D, Ly H, Stepp J. Adv Mater 1998;10: 347–9.
[10] McCarthy PA, Huang JY, Yang SC, Wang HL. Langmuir 2002;18: 259–63.
[11] Li WG, McCarthy PA, Liu DG, Huang JY, Yang SC, Wang HL. Macromolecules 2002;35:9975–82.
[12] Li WG, Hooks DE, Chiarelli P, Jiang YB, Xu HF, Wang HL. Langmuir 2003;19:4639–44.
[13] Cutler C, Bouguettaya M, Reynolds J. Adv Mater 2002;14:684–8.
[14] Groenendaal L, Zotti G, Aubert PH, Waybright SM, Reynolds JR. Adv Mater 2003;15:855–79.
[15] Jonas F, Scharader L. Proceedings of the international conference on science and technology of synthetic metals—ICSM'90; Sep 2–7 1990; Tuebingen, Germany. vol. 41, 1991. p. 831–6.
[16] Heywang G, Jonas F. Adv Mater 1992;4:116–8.
[17] Baur JW, Rubner MF, Reynolds JR, Kim S. Langmuir 1999;15: 6460–9.
[18] Onitsuka O, Fou AC, Ferreira M, Hsieh BR, Rubner MF. J Appl Phys 1996;80:4067–71.
[19] Groenendaal BL, Jonas F, Freitag D, Pielartzik H, Reynolds JR. Adv Mater 2000;12:481–94.
[20] Deleeuw DM, Kraakman PA, Bongaerts PEG, Mutsaers CMJ, Klaassen DBM. Synth Met 1994;66:263–73.
[21] Dietrich M, Heinze J, Heywang G, Jonas F. J Electroanal Chem 1994; 369:87–92.
[22] Winter I, Reese C, Hormes J, Heywang G, Jonas F. Chem Phys 1995; 194:207–13.
[23] Pettersson LAA, Carlsson F, Inganas O, Arwin H. Thin solid films 2nd international conference on spectroscopic ellipsometry (ICSE-2); May 12–15, 1997; Charleston, SC. vol. 313, 1998. p. 356–61.
[24] Aleshin A, Kiebooms R, Menon R, Wudl F, Heeger AJ. Phys Rev B (Condens Matter) 1997;56:3659–63.
[25] Bayer AG. Eur Patent; 1991.
[26] Jonas F, Krafft W, Muys B. Macromolecular symposia 5th European-polymer-federation symposium on polymeric materials (EPF 94). vol. 100, 1995. p. 169–73.
[27] DeLongchamp D, Kastantin M, Hammond P. Chem Mater 2003;15: 1575–86.
[28] DeLongchamp D, Hammond P. Adv Mater 2001;13:1455–9.
[29] Curtis CL, Ritchie JE, Sailor MJ. Science 1993;262:2014–6.
[30] Chiarelli PA, Johal MS, Holmes DJ, Casson JL, Robinson JM, Wang HL. Langmuir 2002;18:168–73.
[31] Chiarelli PA, Johal MS, Casson JL, Roberts JB, Robinson JM, Wang HL. Adv Mater 2001;13:1167–9.
[32] Cho J, Char K, Hong JD, Lee KB. Adv Mater 2001;13:1076–8.
[33] Decher G. Science 1997;277:1232–7.
[34] Decher G, Hong JD, Schmitt J. Thin solid films 5th international conf on Langmuir-Blodgett films. vol. 210, 1992. p. 831–35.
[35] Cheung J, Stockton W, Rubner M. Macromolecules 1997;30:2712–6.
[36] Stejskal J, Trchova M, Fedorova S, Sapurina I, Zemek J. Langmuir 2003;19:3013–8.
[37] Heflin JR, Liu Y, Figura C, Marciu D, Claus RO. Proceedings of the SPIE—the international society for optical engineering conference on nonlinear optical properties of organic materials X. vol. 3147, 1997. p. 10–9.
[38] Shiratori SS, Rubner MF. Macromolecules 2000;33:4213–9.
[39] Mendelsohn JD, Barrett CJ, Chan VV, Pal AJ, Mayes AM, Rubner MF. Langmuir 2000;16:5017–23.
[40] Lvov Y, Yamada S, Kunitake T. Thin Solid Films 1997;300:107–12.
[41] Parikh AN, Allara DL, Azouz IB, Rondelez F. J Phys Chem 1994;98: 7577–90.
[42] Ladam G, Schaad P, Voegel JC, Schaaf P, Decher G, Cuisinier F. Langmuir 2000;16:1249–55.
[43] Johal MS, Casson JL, Chiarelli PA, Liu DG, Shaw JA, Robinson JM, et al. Langmuir 2003;19:8876–81.
[44] Yoo D, Shiratori SS, Rubner MF. Macromolecules 1998;31:4309–18.
[45] Ferreira M, Rubner M. Macromolecules 1995;28:7107–14.